Kemp, D.B., Selby, D., and Izumi, K., 2020, Direct coupling between carbon release and weathering during the Toarcian oceanic anoxic event: Geology, v. 48, https://doi.org/10.1130/G47509.1

SUPPLEMENTAL MATERIAL FOR:

Direct coupling between carbon release and weathering during the Toarcian oceanic anoxic event

David B. Kemp, David Selby, Kentaro Izumi

DESCRIPTION OF METHODS

Rhenium and osmium-isotope analysis

The aim of our Re-Os organic-rich sedimentary rock analysis was to quantify the osmium isotope composition ($^{187}Os/^{188}Os$) of Toarcian seawater. This requires an analytical protocol that extracts and isolates preferentially the hydrogenous rhenium and osmium components from the bulk mudrock sample, whilst minimizing the possibility of liberating and isolating rhenium and osmium present in the detrital mineral (i.e. non-hydrogenous) fraction of the sample. The analytical methods adopted for rhenium and osmium analysis largely followed those of Selby and Creaser (2003), and a summary is provided here. All sample preparation and analysis was carried out at Durham University (UK).

Mudrock samples were ground to a fine powder in an agate pestle and mortar. Between 0.25 and 1 g of powder was digested in a sealed glass Carius tube with an 8 mL solution of 4N H_2SO_4 and 0.25 g/g CrO_3, together with known amount of mixed tracer solution (spike) of ^{185}Re and ^{190}Os. The Carius tubes were then heated gradually to 220°C for 48 hours, after which the tubes were allowed to cool before being opened. Osmium was extracted from the solution using $CHCl_3$, followed by subsequent transfer into HBr. The Os fraction in the HBr solution was then further concentrated by micro-distillation. Rhenium was purified from the remaining CrO_3-H_2SO_4 solution using solvent extraction in a NaOH-C_3H_6O solution, before further purification using anion (single-bead) exchange chromatography. Purified Re and Os were loaded onto Ni and Pt wire filaments, respectively, ready for isotope composition determination using a Thermo Scientific Triton negative thermal-ionization mass spectrometer (NTIMS). Settings used on the Triton for Re and Os analysis were static Faraday collection for Re, and ion-counting using a secondary electron multiplier in peak-hopping mode for Os.

Standard solutions of Re and Os were analyzed along with samples to quantify precision and evaluate reproducibility. Aliquots of our in-house Re and Os standard solutions yielded

$^{185}Re/^{187}Re$ and $^{187}Os/^{188}Os$ values indistinguishable from previously reported values. The measured difference in $^{185}Re/^{187}Re$ values for our standard solution and the accepted $^{185}Re/^{187}Re$ value was used for mass fractionation correction of the Re data from our samples. All Re and Os data were oxide and blank corrected. Procedural blanks for Re and Os were 16.3 ± 5.1 pg/g and 0.09 ± 0.01 pg/g, respectively, with an $^{187}Os/^{188}Os$ value of 0.23 ± 0.03 (N=5).

Uncertainties in our calculated $^{187}Re/^{188}Os$ and $^{187}Os/^{188}Os$ data were quantified using a full propagation of all uncertainties, including those arising from sample weighing, mass spectrometer measurements, spike calibration, blank abundances and reproducibility of the analyzed standards. Uncertainties of all data (1 s.d.) are provided in Table S1.

All data were age corrected to obtain the initial $^{187}Os/^{188}Os$ values of seawater ($^{187}Os/^{188}Os_i$) at the time of sample deposition (182 Ma), based on the following equation:

$$\frac{^{187}Os}{^{188}Os_i} = \frac{^{187}Os}{^{188}Os} - \frac{^{187}Re}{^{188}Os} \cdot \left(e^{(1.666 \times 10^{-11} \cdot age)} - 1\right)$$

where 1.666 x 10^{-11} is the Re decay constant in years, and age is in years (Table S1).

Analytical uncertainty in the calculated $^{187}Os/^{188}Os_i$ was determined by using the square root of the sum of squares approach and includes the uncertainty of the measured $^{187}Re/^{188}Os$ and $^{187}Os/^{188}Os$ ratios and the 0.35% uncertainty of the ^{187}Re decay constant (Smoliar et al., 1996). Although our samples may span a time interval in excess of 5 m.y. (e.g. Ruebsam et al., 2019; Fig. S2), uncertainties in $^{187}Os/^{188}Os_i$ arising from a 6 m.y. maximum probable age differential between the oldest and youngest samples are <0.03, and thus do not significantly affect the trends or absolute values observed in our data.

Elemental analysis

Abundances of Ti, Al and Zr were measured on the same powdered samples used for Re-Os analysis using non-destructive handheld X-ray fluorescence (XRF) analysis following the protocol developed in Saker-Clark et al. (2019). Samples were placed into borosilicate glass vials and covered with x-ray transmissive (low density polyethylene) cling-film. Sample vials were then upturned and placed over the X-ray aperture of an Olympus Delta Premium handheld XRF instrument, held in place in a laboratory stand. Samples were measured in 'Geochem' mode on this instrument using an X-ray exposure time of 120 seconds.

Prior XRF analysis of a set of 30 in-house mudrock standards yielded data that were in excellent agreement with elemental abundances measured on an ICP-MS, based on linear

regression between XRF and ICP-MS values (0.990, 0.975 and 0.995 r^2 values for Ti, Al and Zr, respectively). Nevertheless, the correlations do not define a 1:1 relationship, and XRF values are typically underestimated relative to ICP-MS values. Corrected XRF values can be obtained by adjusting the XRF data using the coefficients of the linear regression (least squares) equations, thus obtaining a 1:1 relationship. The Ti, Al and Zr data of our unknown samples were calibrated to absolute concentrations using the coefficients of the standards. The remaining uncertainty in the data can be quantified as the maximum difference between the XRF data and ICP-MS data of our standards after correction. For Ti, Al and Zr, these maximum uncertainties were 0.03%, 0.89% and 11.1 ppm, respectively. These uncertainties are likely overestimated, since some fraction of the uncertainty for each element stems from analytical errors in the ICP-MS data and not just the XRF. Reproducibility of the XRF data was 2.4%, 4.5% and 1% RSD for Ti, Al and Zr, respectively.

Organic carbon-isotope ($\delta^{13}C_{org}$) analysis

Organic carbon isotope data for 13 of the samples measured for Re-Os analysis had previously been published in Izumi et al. (2012, 2018a, 2018b) and Kemp and Izumi (2014) (data are identified as such in Table S1). The remaining 11 samples were measured for $\delta^{13}C_{org}$ in this study. For these samples, a split of the same powder used for Re-Os and XRF analysis was decalcified in 3M HCl for 24 hours, before washing with de-ionized water until neutrality was reached. Samples were then dried and gently re-crushed in an agate pestle and mortar, before weighing into tin capsules ready for isotope analysis. Samples were measured for organic carbon isotope ratios on a Europa Scientific 20-20 mass spectrometer. Reproducibility was determined by intra-run analysis of a set of in-house standards. Analytical uncertainty (1 s.d.) based on these standards was 0.15‰.

SUPPLEMENTAL FIGURE AND TABLES

Sample ID	Height (m)	[Re] (ppb)	±	[Os] (ppt)	±	[^{192}Os] (ppt)	±	^{187}Re/^{188}Os	±	^{187}Os/^{188}Os	±	rho[1]	%Re blank	%^{187}Os blank	%^{188}Os blank	^{187}Os/^{188}Os$_i$[2]	±	$\delta^{13}C_{org}$	Zr (ppm)	Al (%)	Ti (%)
2016-3AM-2.13	-27.12	3.40	0.01	87.5	0.4	32.0	0.2	211.2	1.2	1.113	0.008	0.657	0.88	0.036	0.202	0.47	0.01	-23.60 [a]	129.09	9.04	0.47
2016-3B-1.04	-22.79	8.94	0.02	237.3	0.9	90.1	0.4	197.3	1.0	0.795	0.005	0.612	0.34	0.018	0.072	0.20	0.01	-24.60 [a]	123.53	9.14	0.47
2010-4-2	-17.02	4.79	0.01	330.4	1.0	132.2	0.6	72.0	0.4	0.374	0.002	0.578	0.251	0.020	0.030	0.15	0.00	-24.69 [b]	130.68	9.93	0.45
2014-4-X1	-14.5	4.64	0.01	329.0	1.1	131.7	0.7	70.0	0.4	0.366	0.003	0.636	0.26	0.021	0.030	0.15	0.00	-24.31 [c]	133.86	9.82	0.45
2013-4-17	-9.47	6.83	0.02	248.3	0.8	96.4	0.4	140.8	0.6	0.611	0.003	0.560	0.176	0.017	0.042	0.18	0.01	-25.13 [b]	132.27	10.73	0.46
2016-5-m0.9	-4.9	5.17	0.01	101.7	0.5	37.0	0.2	277.6	1.4	1.151	0.007	0.607	0.232	0.023	0.108	0.31	0.01	-25.37 [e]	126.71	10.13	0.48
2015-5-m0.53	-4.53	2.85	0.01	70.4	0.5	25.9	0.2	218.7	2.0	1.061	0.013	0.684	0.42	0.036	0.155	0.40	0.02	-26.52 [c]	120.35	9.58	0.45
2015-5-0.78	-3.22	3.02	0.01	95.8	0.6	35.9	0.3	167.2	1.5	0.911	0.011	0.680	0.40	0.031	0.112	0.40	0.02	-26.46 [e]	125.12	9.27	0.47
2014-5-1.83	-2.17	2.36	0.01	70.8	0.5	26.0	0.2	180.8	1.7	1.099	0.014	0.682	0.51	0.035	0.155	0.55	0.02	-27.40 [e]	117.97	9.97	0.41
2015-5-2.10	-1.9	4.63	0.01	104.1	0.5	37.7	0.2	244.4	1.4	1.197	0.009	0.644	0.26	0.022	0.106	0.45	0.01	-27.49 [c]	125.92	9.28	0.45
2014-5-3.49	-0.51	1.10	0.00	29.2	0.2	10.7	0.1	205.9	2.1	1.133	0.015	0.690	1.087	0.083	0.377	0.51	0.02	-27.19 [c]	126.71	11.89	0.58
2013-5-5.45	1.45	1.28	0.00	38.2	0.3	13.9	0.1	182.8	1.8	1.140	0.014	0.688	0.94	0.063	0.289	0.58	0.02	-27.71 [b]	140.22	10.76	0.63
2013-5-6.5	2.5	1.12	0.00	44.8	0.3	16.8	0.2	132.8	1.3	0.919	0.012	0.679	1.07	0.065	0.239	0.52	0.02	-27.35 [c]	132.27	10.02	0.55
2014-S1-X3	5.15	1.51	0.00	45.0	0.2	16.9	0.1	177.0	1.0	0.874	0.006	0.638	0.797	0.067	0.237	0.34	0.01	-27.16 [c]	134.66	10.17	0.50
2013-S2-17	9.6	2.92	0.01	99.0	0.4	37.2	0.2	156.5	0.8	0.892	0.005	0.615	0.410	0.030	0.108	0.42	0.01	-27.58 [c]	135.45	10.41	0.49
2010-8-6	13.9	3.71	0.01	114.1	0.5	42.8	0.2	172.1	1.0	0.893	0.007	0.641	0.32	0.026	0.094	0.37	0.01	-26.04 [c]	119.56	9.41	0.47
2013-10-4 (av.)	20.51	2.70	0.01	63.3	0.4	22.8	0.2	235.8	1.7	1.250	0.012	0.654	0.625	0.032	0.177	0.53	0.02	-23.80 [c]	115.59	9.58	0.46
2013-12-8	25.1	3.73	0.01	85.2	0.4	31.4	0.2	236.4	1.5	1.054	0.007	0.707	1.966	0.081	0.429	0.34	0.01	-23.46 [c]	119.56	9.97	0.44
2010-14-2	32.9	4.13	0.01	81.6	0.4	29.2	0.2	281.5	1.7	1.302	0.010	0.650	0.29	0.026	0.137	0.45	0.01	-23.11 [b]	118.77	9.54	0.45
2010-14-6	36.9	3.01	0.01	78.2	0.3	28.8	0.1	207.4	1.1	1.044	0.006	0.597	0.399	0.033	0.139	0.41	0.01	-23.66 [c]	125.92	10.65	0.47
2010-15-2	39.4	3.25	0.01	92.6	0.4	34.4	0.2	187.7	1.1	0.968	0.006	0.527	0.369	0.030	0.117	0.40	0.01	-23.97 [b]	120.35	8.77	0.35
2010-16-5	48	5.86	0.02	120.8	0.5	44.0	0.2	264.9	1.3	1.155	0.007	0.610	0.205	0.020	0.091	0.35	0.01	-24.87 [c]	116.38	9.25	0.44
2010-18-8.2	64.2	4.21	0.01	121.7	0.5	45.7	0.2	183.0	1.0	0.882	0.006	0.629	0.71	0.032	0.141	0.33	0.01	-23.30 [d]	161.67	11.06	0.65
2010-24-2	90	4.81	0.01	96.2	0.4	34.9	0.2	274.2	1.5	1.176	0.008	0.655	0.62	0.031	0.185	0.34	0.01	-23.39 [d]	128.30	9.15	0.49
2010-10-4 (run 1)		2.63	0.01	60.8	0.4	21.8	0.2	240.0	2.2	1.276	0.016	0.685	0.46	0.036	0.184	0.55	0.02				
2010-10-4 (run 2)		2.77	0.01	65.8	0.3	23.8	0.1	231.7	1.3	1.225	0.008	0.624	0.79	0.028	0.170	0.52	0.01				

[a] Izumi et al. (2018b)
[b] Kemp and Izumi (2014)
[c] This study
[d] Izumi et al. (2012)
[e] Izumi (2018a)
[1] Rho is the associated error correlation function (Ludwig, 1980)
[2] $^{187}Os/^{188}Os_i$ is calculated using a depositional age of 182 Ma (see Methods for details)

Table S1. Full listing of all data. Uncertainties (±) are 2σ standard error, av. = average.

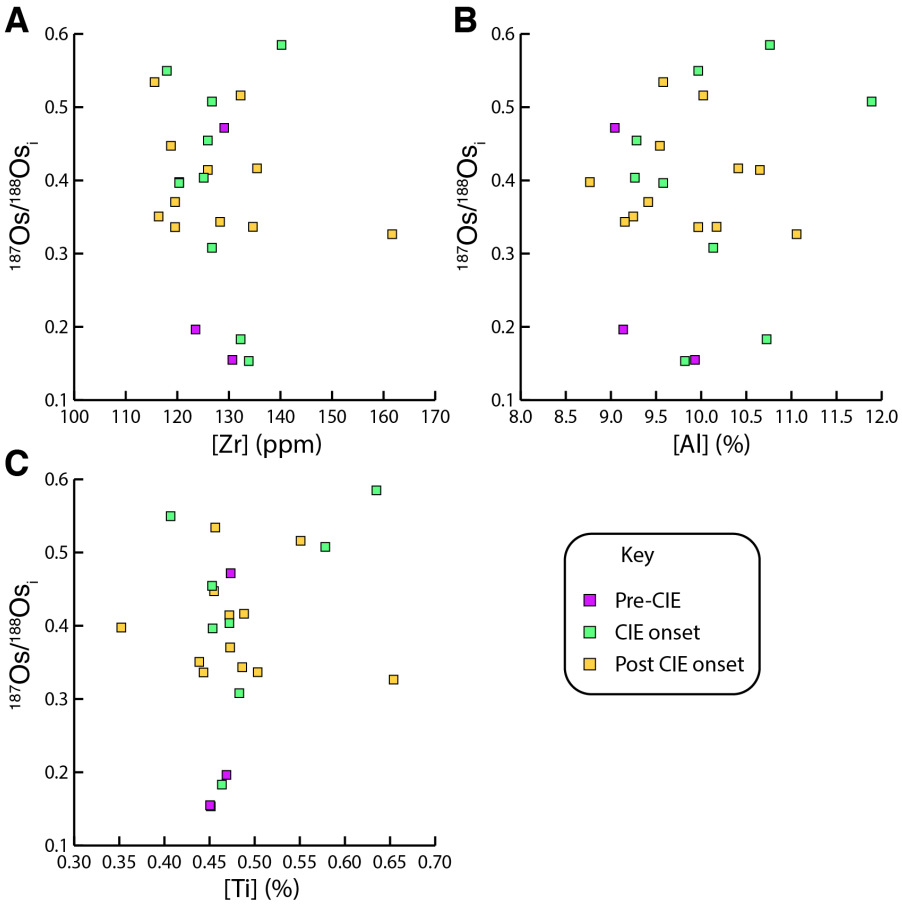

Figure S1. Cross plots of $^{187}Os/^{188}Os_i$ data from Sakuraguchi-dani and elemental proxies for detrital input. The lack of correlation between $^{187}Os/^{188}Os_i$ and these detrital proxies in any part of the CIE (carbon-isotope excursion) emphasizes how changes in $^{187}Os/^{188}Os_i$ in Sakuraguchi-dani reflect changes in hydrogenous osmium (i.e. the global seawater Os inventory), and not localized changes in the isotopic composition of detrital Os delivered to the basin. See Figure 2 of main text for definitions of pre-CIE, CIE onset and Post-CIE onset intervals.

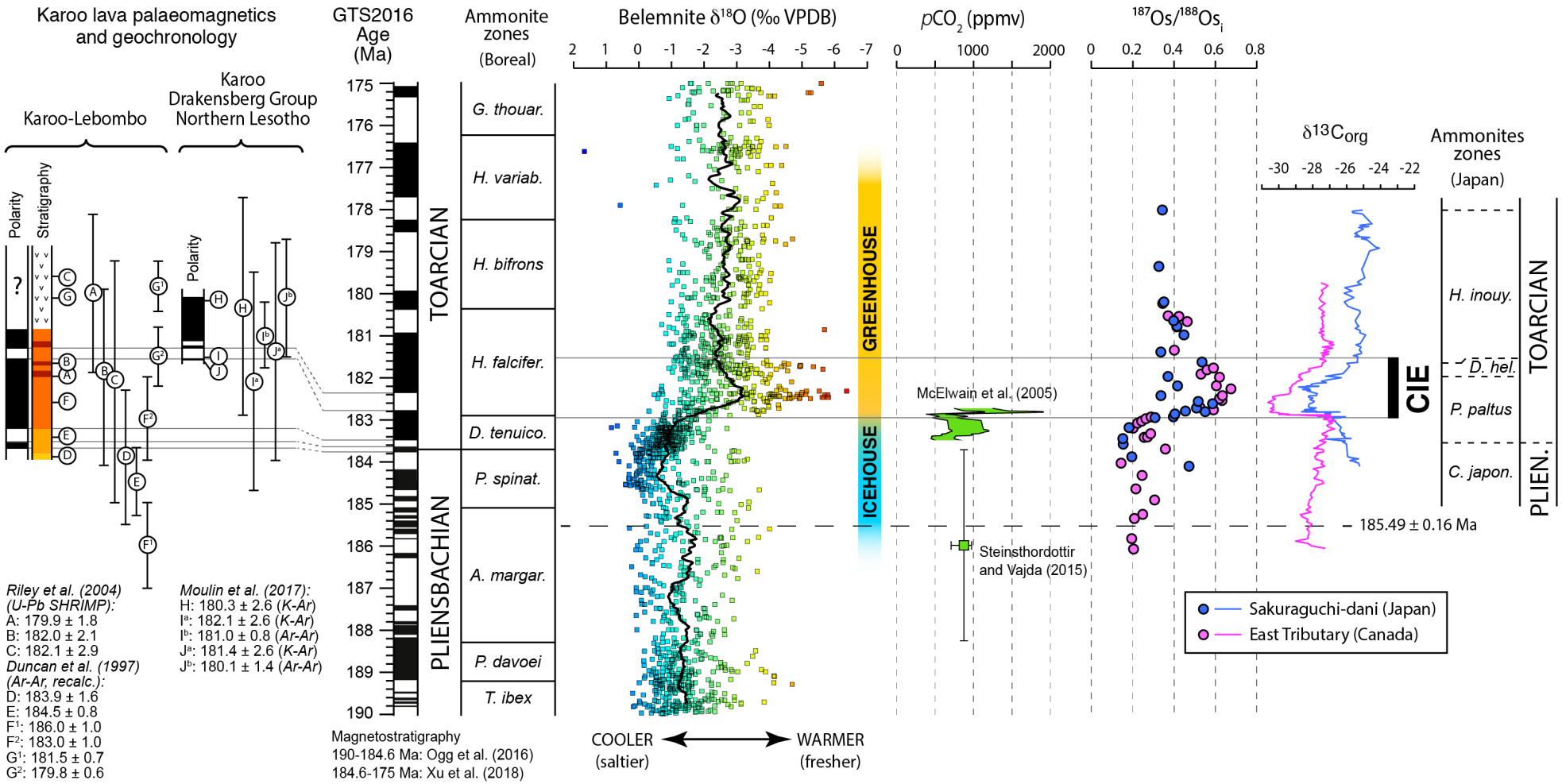
Karoo lava palaeomagnetics and geochronology
Karoo-Lebombo
Karoo Drakensberg Group Northern Lesotho
Polarity
Stratigraphy
Polarity
Riley et al. (2004) (U-Pb SHRIMP):
A: 179.9 ± 1.8
B: 182.0 ± 2.1
C: 182.1 ± 2.9
Duncan et al. (1997) (Ar-Ar, recalc.):
D: 183.9 ± 1.6
E: 184.5 ± 0.8
F¹: 186.0 ± 1.0
F²: 183.0 ± 1.0
G¹: 181.5 ± 0.7
G²: 179.8 ± 0.6
Moulin et al. (2017):
H: 180.3 ± 2.6 (K-Ar)
Iᵃ: 182.1 ± 2.6 (K-Ar)
Iᵇ: 181.0 ± 0.8 (Ar-Ar)
Jᵃ: 181.4 ± 2.6 (K-Ar)
Jᵇ: 180.1 ± 1.4 (Ar-Ar)
GTS2016 Age (Ma)
175
176
177
178
179
180
181
182
183
184
185
186
187
188
189
190
TOARCIAN
PLIENSBACHIAN
Ammonite zones (Boreal)
G. thouar.
H. variab.
H. bifrons
H. falcifer.
D. tenuico.
P. spinat.
A. margar.
P. davoei
T. ibex
Magnetostratigraphy
190-184.6 Ma: Ogg et al. (2016)
184.6-175 Ma: Xu et al. (2018)
Belemnite δ18O (‰ VPDB)
2 1 0 -1 -2 -3 -4 -5 -6 -7
GREENHOUSE
ICEHOUSE
COOLER (saltier)
WARMER (fresher)
pCO2 (ppmv)
0 1000 2000
McElwain et al. (2005)
Steinsthordottir and Vajda (2015)
187Os/188Osi
0 0.2 0.4 0.6 0.8
185.49 ± 0.16 Ma
δ13Corg
-30 -28 -26 -24 -22
CIE
Ammonites zones (Japan)
H. inouy.
D. hel.
P. paltus
C. japon.
TOARCIAN
PLIEN.
Sakuraguchi-dani (Japan)
East Tributary (Canada)

Figure S2. Age calibrated plot of climate indicators, Karoo flood basalt dates and $^{187}Os/^{188}Os_i$ data across the late Pliensbachian and Toarcian. Karoo flood basalt ages and correspondence to palaeomagnetic stratigraphy/lithostratigraphy in the respective sections has been compiled as in Xu et al. (2018). Superscript numbers in lava flow dates indicate different samples from the same level. Superscript letters identify K-Ar (a) or Ar-Ar (b) dating methods, and age uncertainties for all lava dates are 2σ (full details in Xu et al., 2018). Timescale is from Ogg et al., 2016 ('GTS2016'). The magnetostratigraphy for this timescale is taken from Ogg et al. (2016) (190-184.6 Ma), and from Xu et al. (2018) (184.6-175 Ma). Ammonite zonation is from Ogg et al. (2016). The age calibrated belemnite $\delta^{18}O$ compilation (and icehouse-greenhouse interpretation) is from Ruebsam et al. (2019) and references therein. pCO_2 data are based on the stomatal density proxy (references are shown on the figure). The age calibration of the McElwain et al. (2005) pCO_2 data is taken from Ruebsam et al. (2019). The correlation of the Sakuraguchi-dani and East Tributary $^{187}Os/^{188}Os_i$ and $\delta^{13}C_{organic}$ data is based correlating the start and end of the CIE in each section. The $^{187}Os/^{188}Os_i$ and $\delta^{13}C_{organic}$ data are anchored in absolute time using a U-Pb tuff date of 185.49 ± 0.16 Ma (2σ) in the East Tributary section (Them et al., 2017). Data are linearly scaled from this age control point based on available biostratigraphic correlation between Japan and Northern Europe (Nakada and Matsuoka, 2011; updated in Izumi et al., 2018a), and the knowledge that the CIE onset starts just below the base of the *H. falciferum* ammonite Zone in Northern Europe (e.g. Ruebsam et al., 2019; Kemp et al., 2005) and is contemporaneous with the marked decrease in belemnite $\delta^{18}O$ (e.g. Korte and Hesselbo, 2011; Ruebsam et al., 2019). This scaling implicitly assumes a >1 Myr duration for the early Toarcian CIE, in broad agreement with the cyclostratigraphically calibrated duration of Suan et al. (2008), Huang and Hesselbo (2014) and Ruebsam et al. (2014). Note how the pattern of $^{187}Os/^{188}Os_i$ change closely matches belemnite $\delta^{18}O$ (i.e. seawater temperature) and how the shift to higher $^{187}Os/^{188}Os_i$ and lower $\delta^{13}C_{organic}$ is broadly coeval with a sharp increase in pCO_2. Ammonite Zone abbreviations: *thouar. = thouarsense, variab. = variabilis, falcifer. = falciferum, tenuico. = tenuicostatum, spinat. = spinatum, margar. = margaritatus, inouy. = inouyei, hel. = helianthoides, japon. = japonica.*

REFERENCES

Duncan, R.A., Hooper, P.R., Rehacek, J., Marsh, J.S., and Duncan, A.R., 1997, The timing and duration of the Karoo igneous event, southern Gondwana: Journal of Geophysical Research, v. 102, p. 18127-18138.

Huang, C., and Hesselbo, S.P., 2014, Pacing of the Toarcian Oceanic Anoxic Event (Early Jurassic) from astronomical calibration of marine sections: Gondwana Research, v. 25, p. 1348-1356, doi:10.1016/j.gr.2013.06.023.

Izumi, K., Miyaji, T., and Tanabe, K., 2012, Early Toarcian (Early Jurassic) oceanic anoxic event recorded in the shelf deposits in the northwestern Panthalassa: evidence from the Nishinakayama Formation in the Toyora area, west Japan: Palaeogeography, Palaeoclimatology, Palaeoecology, v. 315–316, p. 100-108.

Izumi, K., Kemp, D.B., Itamiya, S., and Inui, M., 2018a, Sedimentary evidence for enhanced hydrological cycling in response to rapid carbon release during the early Toarcian oceanic anoxic event: Earth and Planetary Science Letters, v. 481, p. 162-170.

Izumi, K., Endo, K., Kemp, D.B., and Inui, M., 2018b, Oceanic redox conditions through the late Pliensbachian to early Toarcian on the northwestern Panthalassa margin: Insights from pyrite and geochemical data: Palaeogeography, Palaeoclimatology, Palaeoecology, v. 493, p. 1-10.

Kemp, D.B., Coe, A.L., Cohen, A.S., and Schwark, L., 2005, Astronomical pacing of methane release in the Early Jurassic period: Nature, v. 437, p. 396-399, doi: 10.1038/nature04037.

Kemp, D.B., and Izumi, K., 2014, Multiproxy geochemical analysis of a Panthalassic margin record of the early Toarcian oceanic anoxic event (Toyora area, Japan): Palaeogeography, Palaeoclimatology, Palaeoecology, v. 414, p. 332-341.

Korte, C., and Hesselbo, S.P., 2011, Shallow marine carbon and oxygen isotope and elemental records indicate icehouse-greenhouse cycles during the Early Jurassic: Paleoceanography, v. 26, PA4219, doi:10.1029/2011PA002160.

Ludwig, K.R., 1980, Calculation of uncertainties of U-Pb isotope data: Earth and Planetary Science Letters, v. 46, p. 212-220.

McElwain, J. C., Wade-Murphy, J., and Hesselbo, S. P., 2005, Changes in carbon dioxide during an oceanic anoxic event linked to intrusion into Gondwana coals: Nature, v. 435, p. 479-482.

Moulin, M., Fluteau, F., Courtillot, V., Marsh, J., Delpech, G., Quidelleur, X., and Gérard, M., 2017, Eruptive history of the Karoo lava flows and their impact on early Jurassic environmental change: Journal of Geophysical Research: Solid Earth, v. 122, p. 738-772.

Nakada, K., and Matsuoka, A., 2011, International correlation of the Pliensbachian/Toarcian (Lower Jurassic) ammonoid biostratigraphy of the Nishinakayama Formation in the Toyora Group, southwest Japan: Newsletters on Stratigraphy, v. 44, p. 89-111.

Ogg, J.G, Ogg, G.M, and Gradstein, F.M., 2016, A concise geological timescale: Elsevier, doi:10.1016/B978-0-444-59467-9.00012-1.

Riley, T.R., Millar, I.L., Watkeys, M.K., Curtis, M.L., Leat, P.T., Klausen, M.B., and Fanning, C.M., 2004, U–Pb zircon (SHRIMP) ages for the Lebombo rhyolites, South Africa: refining the duration of Karoo volcanism: Journal of the Geological Society, London, v. 161, p. 547-550.

Ruebsam, W., Mayer, B., and Schwark, L., 2019, Cryosphere carbon dynamics control early Toarcian global warming and sea level evolution: Global and Planetary Change, v. 172, p. 440-453.

Ruebsam, W., Münzberger, P., and Schwark, L., 2014, Chronology of the early Toarcian environmental crisis in the Lorraine Sub-Basin (NE Paris Basin): Earth and Planetary Science Letters, v. 404, p. 273-282.

Saker-Clark, M., Kemp, D.B., and Coe, A.L., 2019, Portable X-Ray fluorescence spectroscopy as a tool for cyclostratigraphy: Geochemistry, Geophysics, Geosystems, v. 20, doi: 10.1029/2018GC007582.

Selby, D., and Creaser, R.A., 2003, Re–Os geochronology of organic rich sediments: an evaluation of organic matter analysis methods: Chemical Geology, v. 200, p. 225-240, doi:10.1016/S0009-2541(03)00199-2.

Smoliar, M. I., Walker, R. J., and Morgan, J. W., 1996, Re-Os ages of Group IIA, IIIA, IVA and IVB iron meteorites: Science, v. 271, p. 1099-1102.

Steinthorsdottir, M., and Vajda, V., 2015, Early Jurassic (late Pliensbachian) CO2 concentrations based on stomatal analysis of fossil conifer leaves from eastern Australia: Gondwana Research, v. 27, p. 932-939.

Suan, G., Pittet, B., Bour, I., Mattioli, E., Duarte, L.V., and Mailliot, S., 2008, Duration of the Early Toarcian carbon isotope excursion deduced from spectral analysis: consequence for its possible causes: Earth and Planetary Science Letters, v. 308, p. 666-679.

Them, T.R., Gill, B.C., Selby, D., Gröcke, D.R., Friedman, R.M., and Owens, J.D., 2017a, Evidence for rapid weathering response to climatic warming during the Toarcian Oceanic Anoxic Event: Scientific Reports, v. 7, doi:10.1038/s41598-017-05307-y.

Xu, W., Mac Niocaill, C., Ruhl, Jenkyns, H.C., Riding, J.B., and Hesselbo, S.P., 2018, Magnetostratigraphy of the Toarcian Stage (Lower Jurassic) of the Llanbedr (Mochras Farm) Borehole, Wales: basis for a global standard and implications for volcanic forcing of palaeoenvironmental change: Journal of the Geological Society (London), v. 175, p. 594-604, doi:10.1144/jgs2017-120.